energies

MDPI

Article

Pore Structure Characteristics and Influencing Factors of Tight Reservoirs Controlled by Different Provenance Systems: A Case Study of the Chang 7 Members in Heshui and Xin'anbian of the Ordos Basin

Ling Xiao [1,2], Ling Bi [1,2], Tao Yi [3], Yutian Lei [3] and Qinlian Wei [1,2,4,*]

[1] School of Earth Science and Engineering, Xi'an Shiyou University, No.18 2th Dianzi Road, Yanta District, Xi'an 710065, China
[2] Shaanxi Key Laboratory of Petroleum Accumulation Geology, Xi'an Shiyou University, Xi'an 710065, China
[3] No. 12 Oil Production Plant, PetroChina Changqing Oilfield Company, Heshui, Qingyang 745400, China
[4] Department of Geology, University of Regina, Regina, SK S4S 0A2, Canada
* Correspondence: wql@xsyu.edu.cn

Abstract: The evaluation of pore structure is critical in understanding reservoir characteristics. This study aims to analyze the microscopic pore structure characteristics of tight reservoirs from various provenances through physical property analysis, casting thin sections, scanning electron microscopy (SEM), and constant−rate mercury injection. The pore throat parameters of the Chang 7 reservoir were analyzed and compared to those of the Xin'anbian and the Heshui areas. The results show that intergranular pores dominate the pore type of the Chang 7 reservoir in the Xin'anbian area, followed by feldspathic dissolution pores, with high-necked and tubular throat content caused by weak compaction and dissolution, respectively. On the other hand, feldspar dissolution pores dominate the pore type of the Chang 7 reservoir in the Heshui area, followed by intergranular pores, with a high content of tube−bundle throats caused by dissolution and flake−bent flake throats caused by compaction. The difference in pore parameters between the two blocks is minimal, but the difference in throat parameters is significant. Under the same permeability conditions, the throat radius distribution range of the Chang 7 reservoir samples in the Heshui area is narrower than that in the Xin'anbian area, with tiny throats contributing significantly to reservoir permeability. Sedimentary hydrodynamic conditions and diagenesis are the primary reasons for the differences in the pores, throats, and pore structure parameters of the Chang 7 tight reservoirs.

Keywords: pore type; pore throat parameter; pore structure; tight reservoir; Ordos Basin

Citation: Xiao, L.; Bi, L.; Yi, T.; Lei, Y.; Wei, Q. Pore Structure Characteristics and Influencing Factors of Tight Reservoirs Controlled by Different Provenance Systems: A Case Study of the Chang 7 Members in Heshui and Xin'anbian of the Ordos Basin. *Energies* **2023**, *16*, 3410. https://doi.org/10.3390/en16083410

Academic Editors: Kelai Xi and Tian Yang

Received: 10 March 2023
Revised: 1 April 2023
Accepted: 11 April 2023
Published: 13 April 2023

1. Introduction

In recent years, unconventional oil and gas exploration and development have become essential components of global oil and gas production [1,2]. Significant advances have been made in unconventional oil and gas, particularly in the depositional models of fine−grained sedimentary rocks, the characterization of micro−nano pore throats, the prediction of "sweet spots", and the evaluation parameters of unconventional oil and gas [3]. However, the Chang 7 tight−oil reservoir presents challenges to effective development due to its rapid lithology changes, poor continuity, significant heterogeneity, and varied oil content, which can affect reservoir development [4–7]. The pore structure of tight reservoirs varies due to differences in sedimentary background and diagenetic processes, and even reservoirs with similar permeability may have vastly different pore structure parameters. Therefore, changes in reservoir physical properties are closely linked to changes in the pore structure [8]. While numerous publications exist on the tight−oil reservoir of the Chang 7 member in the Ordos Basin, including om the sedimentary characteristics [9–12], the reservoir characteristics [13], and hydrocarbon accumulation [14–17], there is a need for

further discussion on the differences in the pore structure characteristics of tight reservoirs and their controlling factors under different provenances.

The primary objective of this study is to investigate the differences in pore structure characteristics of the Chang 7 tight reservoir in the Xin'anbian and Heshui areas under different provenances using casting thin sections, scanning electron microscopy (SEM), petrophysical properties, and constant−rate mercury intrusion (CRMI). Additionally, the study aims to identify the causes of these differences. The research findings will have significant implications for forecasting and optimizing the "sweet spot" of tight reservoirs, executing effective differential development techniques, and devising pertinent policies.

2. Geological Background

During the Late Triassic, the Ordos Basin was a vast continental depression lake basin that accumulated terrigenous clastic rocks dominated by fluvial–lacustrine deposits with a thickness of approximately 1000–1500 m [18]. The Yanchang Formation can be subdivided into ten members, from Chang 1 to Chang 10 [18]. The Chang 7 member represents the peak of lake development, with the most extensive water body area and the deepest water depth, and covers an area of approximately 5.6 × 10^4 km^2. The sedimentary rocks deposited during this period were fine−grained and rich in organic matter. Semi−deep and deep lakes are distributed in the southwestern part of the basin (Figure 1).

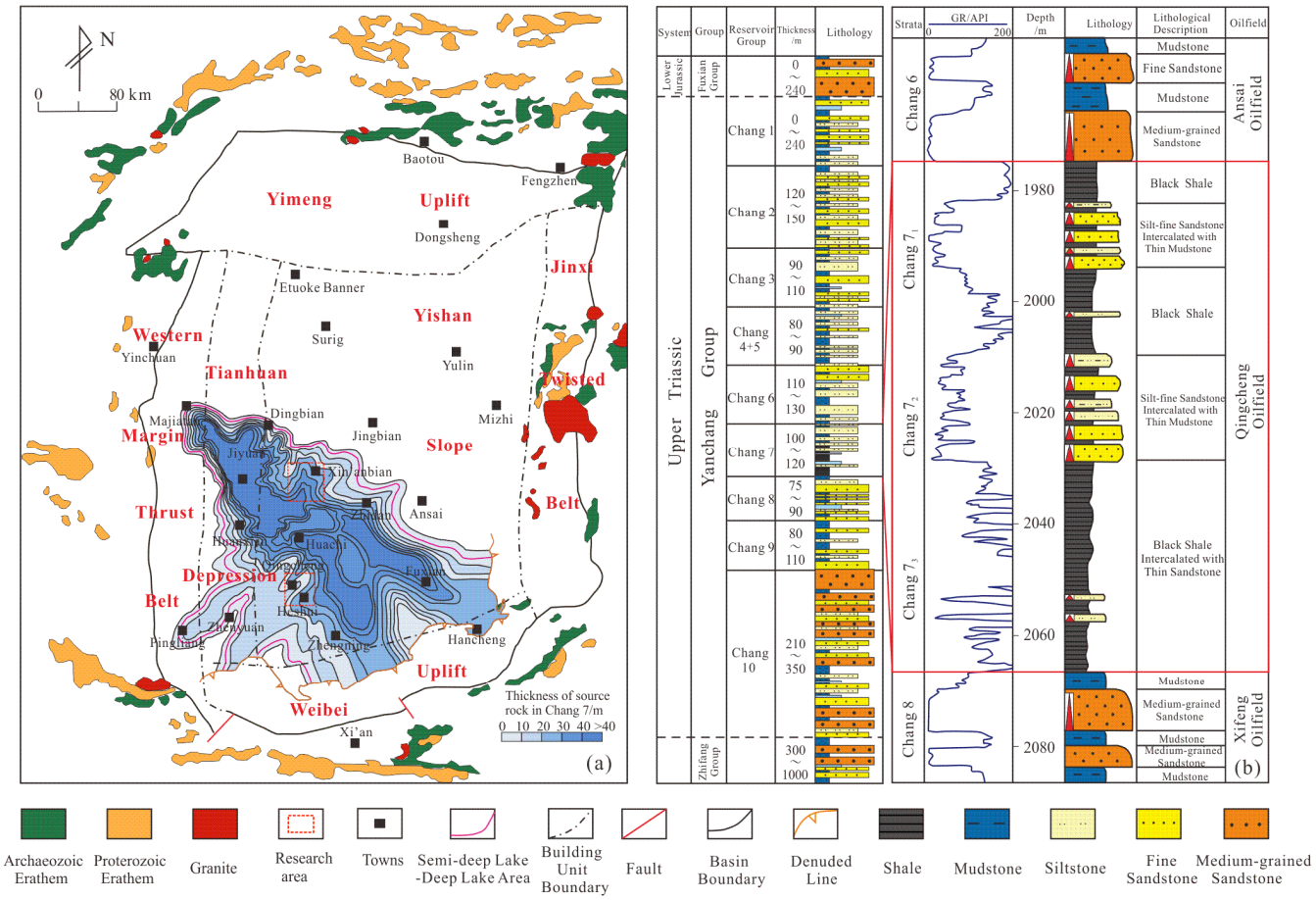

Figure 1. Location of the research area (**a**) and target horizon (**b**).

During the deposition of the Chang 7 member, multiple provenance areas developed and a lake−delta sedimentary system was formed. The Xin'anbian area is northwest of the Yi−Shaan slope (Figure 1). Controlled by a provenance to the northeast, a set of meandering river delta front subfacies deposits developed in the Chang 7 reservoir [6]. The primary reservoir sand body type is an underwater distributary channel. The average thickness of the sand body is 28.5 m, and the average thickness of the oil layer is 12.2 m.

The Heshui area is southwest of the Yishan slope (Figure 1). The Chang 7 reservoir in this region is controlled by provenance in the southwest, and gravity flow deposits are developed. The primary reservoir sand body type is sandy debris flow, with an average sand body thickness of 16.4 m and an average buried depth of the reservoir of 2050 m [6].

3. Methodology

This study employed several techniques to analyze the pore structure of tight reservoirs including: thin−section casting; scanning electron microscopy (SEM); rock physical property tests, including tests for porosity and permeability; and CRMI. The authors utilized 459 casting thin sections and 3 SEM results to determine the reservoir's mineral composition and pore types. The quality of the reservoir was assessed based on the results of 995 rock physical property tests. Additionally, the study investigated the effect of microporous throat structure on the permeability of tight sandstone using a comprehensive approach that included casting thin sections, SEM, and CRMI.

The Shaanxi Key Laboratory of Oil and Gas at Xi'an Shiyou University conducted the rock physical property tests, casting thin sections, and SEM analysis, while the China Petroleum Exploration and Development Research Institute conducted the CRMI. The CMS−300, which utilizes helium and nitrogen as working media with a pressure sensor accuracy of 0.1%, was used to determine the petrophysical properties of the rocks. The Aspe−730 mercury porosimeter from Coretest Systems, located in New Jersey, USA, was used to conduct constant−rate mercury intrusion (CRMI) with a minimum detectable throat radius of 0.1 μm.

4. Results

4.1. Differences in Rock Types

The reservoir sandstones of Chang 7 in the Xin'anbian area consist of fine gray−gray−black sandstones. Thin section analysis of 221 samples revealed that the sandstone reservoir rock types are classified as arkose, followed by lithic arkose (Figure 2). The average quartz content is 26.4%, the feldspar content is 41.3%, and the rock debris content is 16.4% (Figure 3a). The primary lithology of the reservoir sandstone in the Heshui area is gray−black fine siltstone and fine sandstone. Analysis of 238 samples from casting thin sections showed that the rock types are classified as lithic feldspar sandstone and feldspathic litharenite, with some arkose sandstone (Figure 2). The detrital component has an average quartz content of 39.6%, an average feldspar content of 22.7%, and an average rock debris content of 21.9% (Figure 3b).

Overall, the quartz and rock debris content of the reservoirs in Xin'anbian are lower than those in Heshui, but the feldspar content is higher than that in the Heshui area (Figure 3a). The content of metamorphic rock fragments in the Xin'anbian area is lower than in the Heshui area (Figure 3b). In comparison, the igneous and sedimentary rock debris content is higher than that in the Heshui area, which is mainly related to the properties of rocks from different provenance directions.

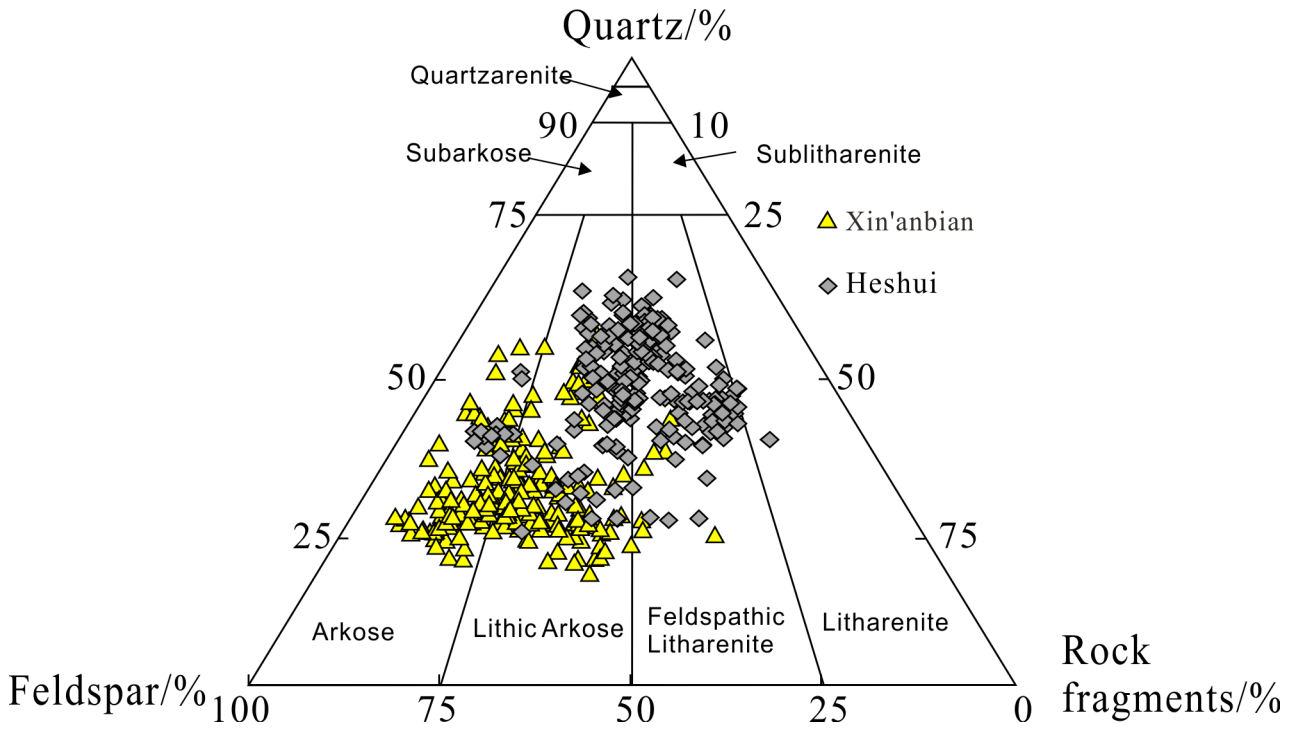

Figure 2. Ternary diagram of Chang 7 sandstone composition in the Xin'anbian area and the Heshui area, Ordos Basin.

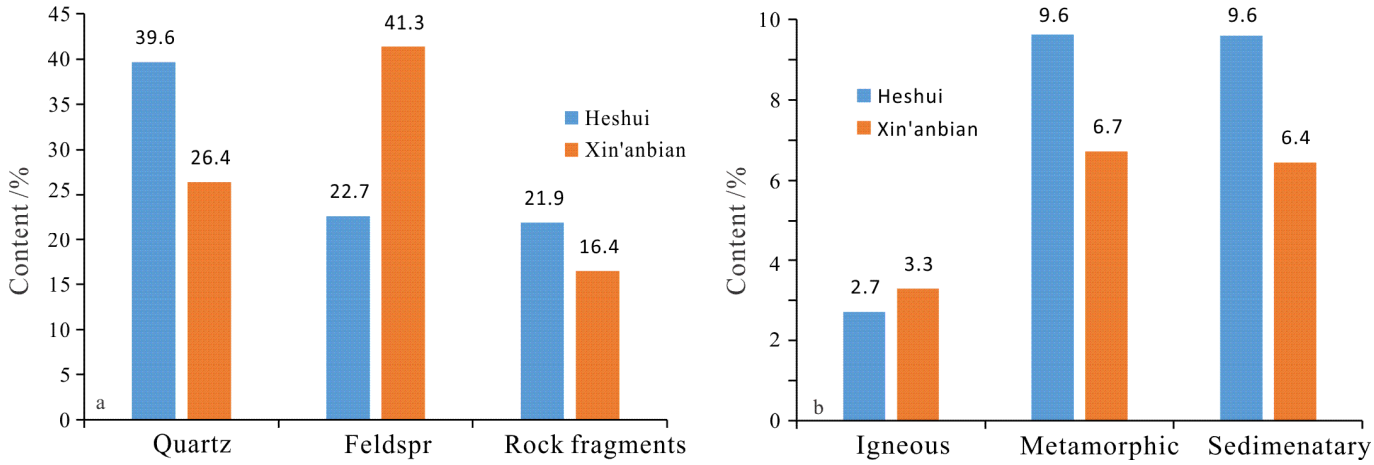

Figure 3. Histogram of sandstone particle composition. (**a**) Main mineral composition of particles; (**b**) Debris composition.

4.2. Differences in the Types of Fillers

The dominant cement in the interstitial material of the reservoir in the Xin'anbian area is chlorite (3.82%), followed by ferrocalcite (3.10%), kaolinite (2.44%), illite (2.17%), and siliceous (1.06%) (Table 1) (Figure 4a), among others. In contrast, the material with the highest average content in the reservoir interstitials in the Heshui area is illite (8.88%), followed by iron calcite (1.53%), iron dolomite (1.22%), and siliceous (1.03%) (Table 1) (Figure 4a). Overall, the content of interstitial materials in Xin'anbian is lower than in Heshui (Figure 4b). In general, the content of fillings in Xin'anbian is lower than in Heshui (Figure 4b), and the chlorite and kaolinite content in Xin'anbian is much higher than that in Heshui (Figure 4a). Chlorite appears as a pore−scale edge, which has an excellent anti−compaction effect, increasing the content of intergranular pores and necked throats caused by weak compaction in the Xin'anbian area compared to that in the Heshui area. The

high illite content in the Heshui area, accounting for more than 50% of the total interstitial content, is filled between the pores in the form of silk strands, resulting in shrinkage and blockage of the pores and throats, which makes it easy for various complex pipe bundle throats to form.

Table 1. Statistics of filler contents of the Chang 7 reservoir in the Xin'anbian area and the Heshui area, Ordos Basin.

Cements	Heshui	Xin'anbian
Illite/%	8.88	2.17
Chlorite/%	0.79	3.82
Kaolinite/%	0.06	2.44
Reticulated Clay/%	0.02	0.38
Calcite/%	0.11	0.25
Ferric Calcite/%	1.53	3.10
Dolomite/%	0.01	0.05
Ferric Dolomite/%	1.22	0.07
Siliceous/%	1.03	1.06
Feldspar/%	0.07	0.08
Other Fillers/%	0.09	0.02
Total/%	13.81	13.62
Number of Samples	238	221

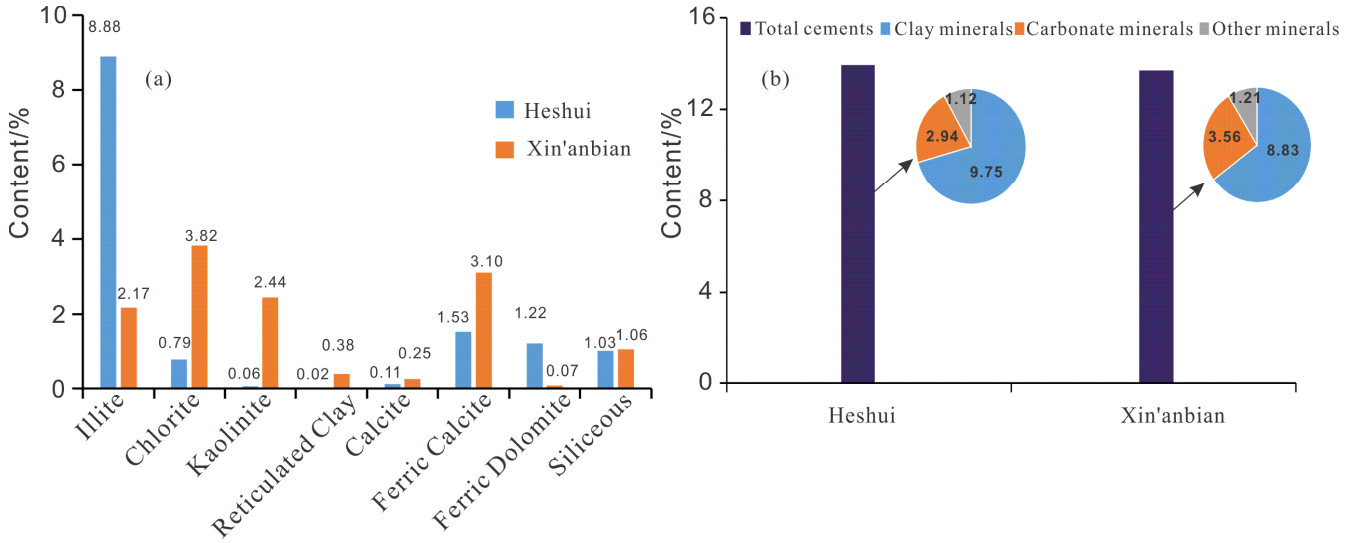

Figure 4. Contents and types of cement (**a**) and total cements (**b**) in Heshui and Xin'anbian.

4.3. Difference in Physical Properties

Tight reservoirs can be classified based on their porosity and permeability characteristics. A porosity greater than 15% is classified as medium porosity, while a porosity between 10–15% is classified as low porosity. Additionally, porosities between 5–10% and less than 5% are categorized as ultra−low porosity. On the other hand, super low permeability is characterized by a permeability range of 1–10 mD, while permeability of less than 0.1 mD is classified as ultra−low permeability (Figure 5c) [1]. An analysis of the physical properties of 411 samples from the Chang 7 tight reservoir in Xin'anbian indicated that most samples have a porosity between 4.0% and 15.78%, with an average of 7.99% (Figure 5a,b). The porosity distribution displayed clear patterns, with a vast majority of ultra−low and super−low porosity samples accounting for 90% of the total. Conversely, a few samples displayed low porosity, representing only 10% of the total (Figure 5c). Regarding permeability, most samples fell within the range of 0.0101 mD to 10.0 mD, with an average of 0.281 mD. Over 99% of the samples exhibited permeability values below 1 mD, with only 0.97% showing a permeability value greater than 1 mD (Figure 5c).

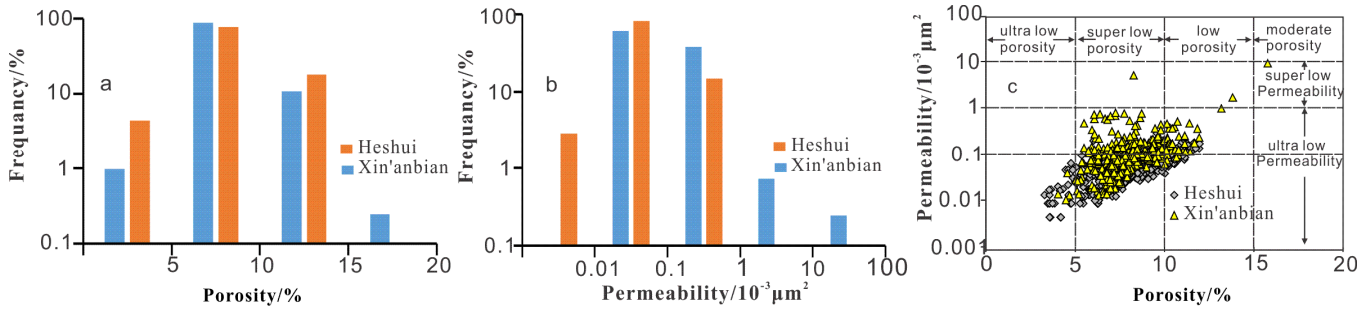

Figure 5. Physical characteristics of Chang 7 tight reservoir in the Xin'anbian area and the Heshui area, Ordos Basin. (**a**) Porosity histogram; (**b**) Permeability histogram; (**c**) The Intersection Diagram of Porosity and Permeability.

Similarly, the physical property analysis of 584 samples from the Chang 7 tight reservoir in the Heshui area showed that the porosity is mainly in the range of 3.29–11.97%, with an average of 8.33% (Figure 5a,b). There were many ultra−low and super−low porosity samples, accounting for 81.9% of the total, while the number of low porosity samples was 18.1%. The permeability ranged primarily from 0.0041 mD to 0.3825 mD, with an average of 0.059 mD. In this case, all sample permeability values were below 1 mD, accounting for 100% of the total samples (Figure 5c).

Overall, the Chang 7 tight reservoirs in Xin'anbian and Heshui areas are ultra−low porosity−ultra−low permeability reservoirs (Figure 5c). The porosity value of the Xin'anbian area is lower than that of the Heshui area, but its permeability is higher than that of the Heshui area. However, the relationship between porosity and permeability in the Xin'anbian area is relatively scattered, possibly due to fractures (Figure 5c).

4.4. Differences in Pore Structure

4.4.1. Differences in Pore Type

Utilizing SEM, researchers can obtain crucial information regarding the morphology and structure of the sample surface. This technique allows for pore shape, size and distribution to be observed, and for statistical analysis of pore types, including circular, elliptical, rectangular, and irregular shapes, to be carried out. Additionally, by examining the cross−section of a casting thin section through an optical microscope, researchers can obtain more detailed pore information, such as pore location, shape, size, and origin, facilitating statistics on pore types [1–3,19].

To calculate the surface porosity, researchers can use the formula: surface porosity = (pore area/total area) × 100%. The pore area refers to the total area of all pores in the casting thin section, while the total area refers to the area of the entire casting thin section. The pore area can be measured by using computer software or manual measurements. Based on SEM and casting thin section observations, the primary pore types in the tight reservoirs of the Xin'anbian area are intergranular pores and feldspar dissolution pores, with a smaller number of cutting dissolution holes, intercrystalline pores, and microcracks (Table 2). The surface porosity of the Xin'anbian tight reservoir is 2.79%, with intergranular pores being the most common pore type, accounting for 41.5% of total pores, followed by feldspar dissolution pores, which account for 41.2% of total pores.

Table 2. Comparison of content of different pore types of the Chang 7 tight reservoirs in the Xin'anbian area and the Heshui area, Ordos Basin.

Research Area	Absolute Content of Pore Types/%					Surface Porosity(%)	Number of Samples
	Intergranular Pores	Feldspar Dissolved Pores	Lithic Dissolved Pores	Intercrystalline Pores	Micro-Cracks		
Xin'anbian	1.16	1.15	0.21	0.07	0.04	2.79	221
Heshui	0.34	1.01	0.10	0.01	0.01	1.57	238

In comparison, the dominant pore types in the tight reservoirs of the Heshui area are feldspar dissolution pores and intergranular pores, with a few lithic dissolved pores, intercrystalline pores, and micro−cracks (Table 2). The surface porosity of the Heshui tight reservoir is 1.57%, with feldspar dissolution pores being the most prevalent, accounting for 64.3% of total pores, followed by intergranular, accounting for 21.6% of total pores.

Although the surface porosity of both areas is relatively low, the Xin'anbian area has a higher surface porosity than the Heshui area and a greater variety of pore types, including a higher percentage of intergranular pores.

4.4.2. Differences in Throat Type

According to the classification scheme of sandstone throat types by Luo Zhetan and Wang Yuncheng [19], combined with the differences in reservoir transformation caused by different diagenesis, we analyzed the throat types of the Chang 7 tight reservoirs in the Xin'anbian and Heshui areas.

The throat types of the tight reservoirs in these two areas mainly include neck-shaped throats caused by weak compaction, sheet-shaped and curved sheet-shaped throats caused by compaction, tube-bundle throats caused by dissolution, and clay mineral tubular throats of cemented origin.

Neck−shaped throats caused by inadequate compaction of the tight reservoir in the Xin'anbian area are the most developed. Chlorite film filled at the edge of clastic particles protects the original intergranular pores after compaction [20], with a throat radius generally greater than 2.0 μm (Figure 6a).

The tube−like throats formed via dissolution are the second most abundant type by content. The radius of these throat is typically tiny, measuring less than 2.0 μm (Figure 6b).

The content of sheet−like and curved sheet-like throats caused by compaction ranks third. Under strong compaction, the grains are mainly in line contact and arranged in one direction, making the radius of this type of throat smaller, generally at 1~0.5 μm (Figure 6h).

The tube−like throats caused by clay mineral cementation rank fourth in content. This throat type mainly appears in the intercrystalline pore development area, and the throats are tiny, most being smaller than 0.5 μm (Figure 6c).

In the Heshui area, dissolution pores are well−developed, and the bundle−like throats formed by dissolution are the most abundant. Although these throats vary in size and exhibit substantial heterogeneity, they are numerous (Figure 6e), making them the most prevalent throat type. The content of throats caused by compaction ranks second, and the throat radius of this type of throat is generally less than 1.5 μm (Figure 6g,i). The third most abundant throat type is the constricted throat caused by inadequate compaction. Although the radius of such throats is relatively large, there are relatively few of them (Figure 6d). The bundle−like throats of clay mineral cementation origin are the fourth most abundant type (Figure 6f).

Overall, the neck−shaped throat caused by weak compaction and the tubular throat caused by clay mineral cementation in the Xin'anbian area are more developed than those in the Heshui area. In contrast, the bundle−like throat formed by dissolution and the flaky curved throat caused by compaction in the Heshui area are more developed than those in the Xin'anbian area. Therefore, the type of pore throat in the Heshui area is more complex than that in the Xin'anbian area.

4.4.3. Differences in Pore and Throat Characteristics

Pore and throat characteristics can be quantified using constant−rate mercury injection (CRMI) pressure fluctuation measurements [21,22]. This method can measure the total volume of pores and throats at a certain throat level and calculate the number of throats at this level to determine the permeability contribution of different throats. To comprehensively consider the sedimentary background, physical properties, and oil−bearing characteristics, seven samples were selected from the Xin'anbian area, and eleven samples were selected from the Heshui area for CRMI experiments. For ease of comparative analysis, the

18 samples were classified according to their permeability (Table 3). Type a samples have a permeability greater than 0.1×10^{-3} μm^2, type b samples have a permeability ranging from 0.05×10^{-3} μm^2 to 0.1×10^{-3} μm^2, and type c samples have a permeability less than 0.05×10^{-3} μm^2. Representative samples were selected for the three types from different research areas. The permeability of the representative samples of type a was 0.12×10^{-3} μm^2 (Xin'anbian) and 0.101×10^{-3} μm^2 (Heshui area). The permeability of the representative samples of type b was 0.06×10^{-3} μm^2 (Xin'anbian) and 0.06×10^{-3} μm^2 (Heshui area). Finally, the permeability of the representative samples of type c was 0.025×10^{-3} μm^2 (Xin'anbian) and 0.027×10^{-3} μm^2 (Heshui area).

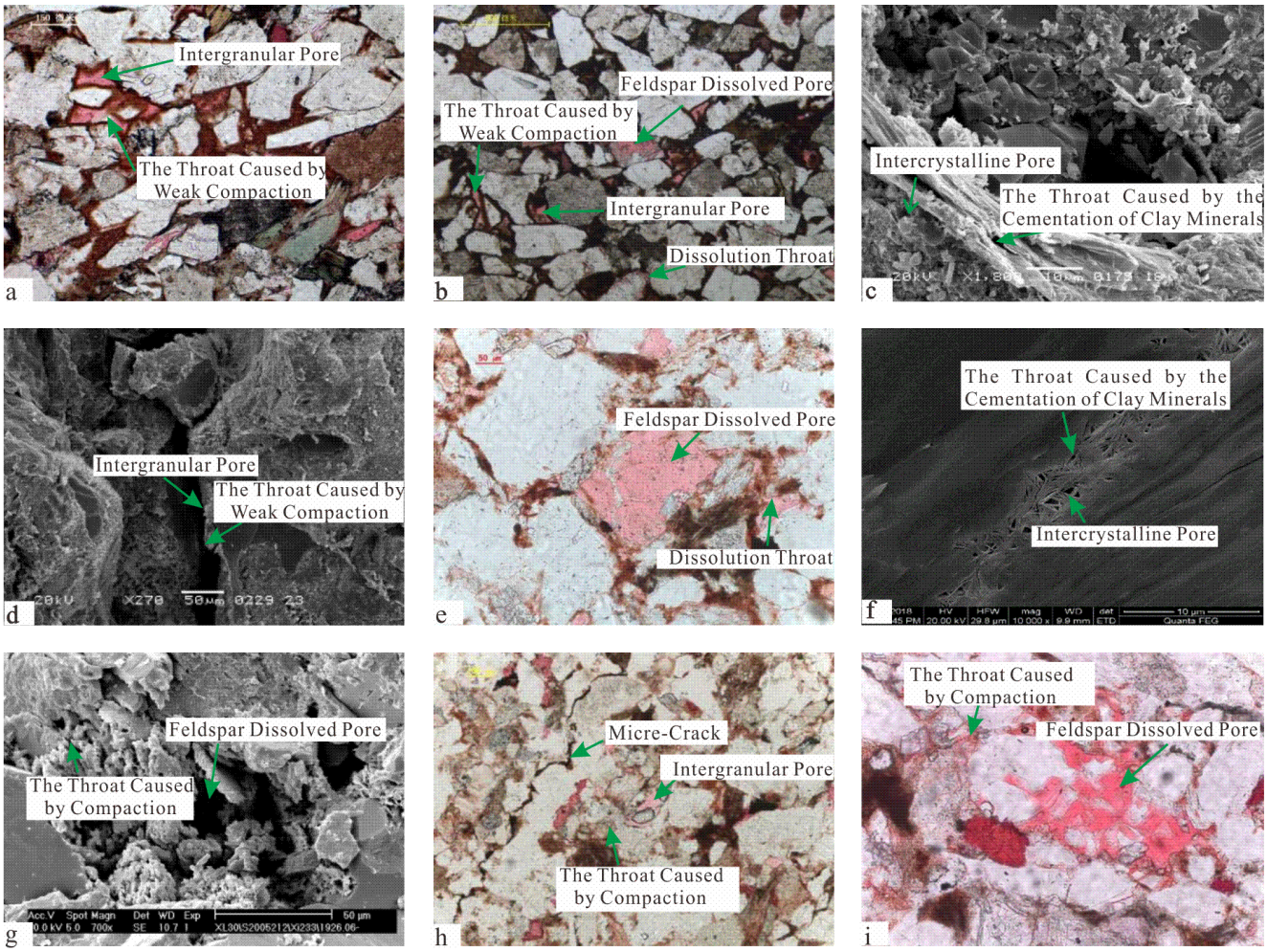

Figure 6. Main pore throat types of Chang 7 tight reservoir in the Xin'anbian area and the Heshui area, Ordos Basin. (**a**) Well A92, 2297.67 m, Intergranular Pore, Feldspar Dissolved Pore, Throat Caused by Weak Compaction; (**b**) Well Y149, 2173.5 m, Intergranular Pore, Feldspar Dissolved Pore, Throat Caused by Weak Compaction; (**c**) Well G58, 2453.0 m, Intercrystalline Pore, Throat Caused by the Cementation of Clay Minerals; (**d**) Well J46, 2279.9 m, Intergranular Pore, Throat Caused by Weak Compaction; (**e**) N11, 1385.9 m, Feldspar Dissolved Pore, Dissolution Throat; (**f**) Z47, 1948.8 m, Intercrystalline Pore, Throat Caused by the Cementation of Clay Minerals; (**g**) Well X233, 1926.06 m, Feldspar Dissolved Pore, Dissolution Throat; (**h**) C95, 1979.1 m, Intergranular Pore, Throat Caused by Compaction, Micre−crack; (**i**) X80, 1834.9 m, Feldspar Dissolved Pore, Dissolution Throat, Throat Caused by Compaction.

Table 3. Sample statistics of CRMI of Chang 7 reservoir.

Type	Search Area	Sample Serial Number	Porosity/%	Permeability/ (10^{-3} μm^2)	Lithology	Note
a	Xin'anbian	Y263	9.1	0.121	Grey Fine Sandstone	Representative Sample
		G184	10.2	0.154	Grey Fine Sandstone	
	Heshui	X1	12.30	0.101	Grey-black Silt-fine Sandstone	Representative Sample
		X271	9.81	0.103	Grey-black Silt-fine Sandstone	
b	Xin'anbian	J46	9.14	0.052	Grey Silt-fine Sandstone	
		J46	10.08	0.098	Grey-black Silt-fine Sandstone	
		L50	7.8	0.06	Grey-black Silt-fine Sandstone	Representative Sample
	Heshui	C98	9.78	0.060	Grey-black Fine-silt Sandstone	Representative Sample
		N148	10.17	0.051	Grey-black Fine-silt Sandstone	
c	Xin'anbian	B89	9.06	0.025	Grey-black Fine-silt Sandstone	Representative Sample
		A83	9.54	0.046	Grey-black Fine-silt Sandstone	
	Heshui	Y76	7.61	0.018	Grey-black Fine-silt Sandstone	
		L17	7.72	0.020	Grey-black Fine-silt Sandstone	
		M53	8.17	0.027	Grey-black Fine-silt Sandstone	Representative Sample
		Z180	7.27	0.029	Grey-black Fine-silt Sandstone	
		X271	8.57	0.035	Grey-black Fine-silt Sandstone	
		L338	5.25	0.033	Grey-black Fine-silt Sandstone	
		N105	3.72	0.0023	Grey-black Fine-silt Sandstone	

4.4.4. Differences in Pore Parameters

The results of the CRMI test revealed that the pore radii of seven samples in the Xin'anbian area range between 100 μm and 220 μm, with an average pore radius ranging from 138.98 to 161.47 μm. Meanwhile, the pore radii of eleven samples in the Heshui area ranged from 80 to 240 μm, with an average pore radius ranging from 126.56 to 154.72 μm (Figure 7). The distribution range of pore radius in the reservoir of the Heshui area is broader than that of the Xin'anbian area, which may be directly related to the higher content of feldspar dissolution pores, especially feldspar mold pores in the Heshui area (Figure 7a,b).

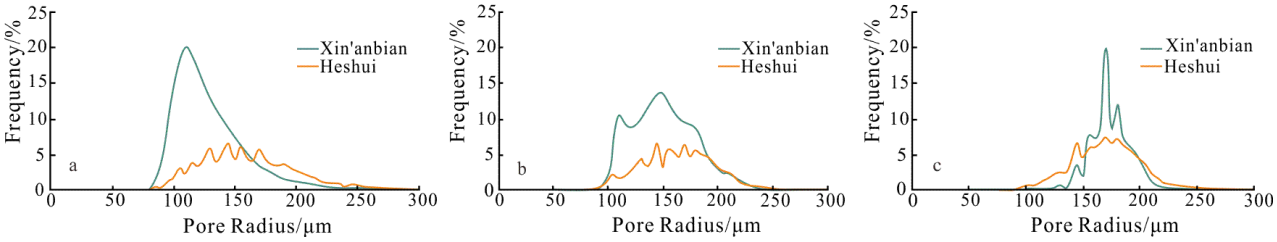

Figure 7. Pore size distribution of different types of pore structure of Chang 7 tight reservoir in the Xin'anbian area and the Heshui area, Ordos Basin. (**a**) Distribution of pore radius for a pore structure of Type a; (**b**) Distribution of pore radius for a pore structure of Type b; (**c**) Distribution of pore radius for a pore structure of Type c.

The analysis of the three types of samples with the same permeability indicates that there is little difference in the distribution range of pore radius (Figure 7). However, the peak size and position are different. Through comparison, it can be found that among the three types of representative samples, the peak position of the pore radius samples from the Xin'anbian area in type c is to the right of the peak position for those from the Heshui area. Additionally, the peak is higher than type a and type b (Figure 7c). This observation indicates that in the case of similar permeability, the characteristics of pore radius are related to porosity. Specifically, the larger the porosity, the further the peak position of the pore radius moves to the right.

4.4.5. Differences in Throat Parameters

Analysis of three types of samples with varying permeability revealed that the throat distribution range in the Xin'anbian area is between 0.1 and 0.8 μm (Type a), 0.1 and 0.5 μm (Type b), and 0.1 and 0.6 μm (type c), whereas in the Heshui area it ranges between 0.1 and 0.5 μm (type a), 0.1 and 0.4 μm (type b), and 0.05 and 0.4 μm (Type c) (Figure 8). At the same level of permeability, the throat radius of tight−oil reservoirs in the Xin'anbian area is more widely distributed than in the Heshui area. The peak value of throat radius in the Xin'anbian area is skewed to the right, indicating that larger throats are more developed in the Xin'anbian area than in the Heshui area, possibly due to the development of neck−shaped throats caused by weak compaction in the Xin'anbian reservoir (Figure 8a,b). However, as permeability decreases, the difference in throat radius distribution between the two regions becomes smaller (Figure 8c) due to the decrease in intergranular pores of chlorite pores, which have the critical anti-compaction ability, and an increase in tubular throats formed by dissolution and clay mineral cementation.

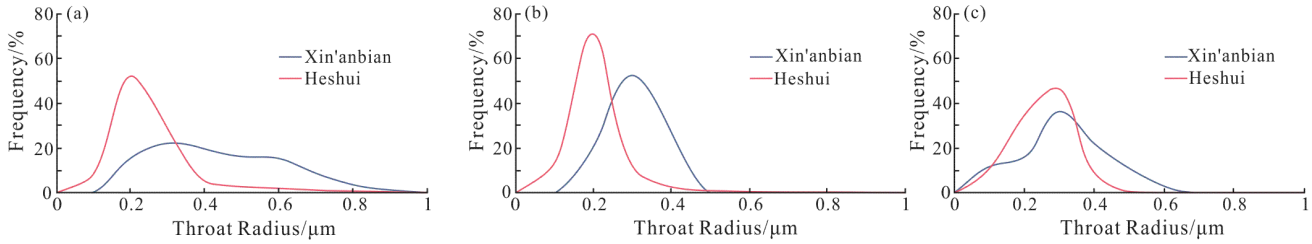

Figure 8. Throat size distribution of different types of pore structure of Chang 7 tight reservoir. (**a**) Distribution of throat radius for a pore structure of Type a; (**b**) Distribution of throat radius of for a pore structure of Type b; (**c**) Distribution of throat radius for a pore structure of Type c.

4.4.6. Differences in Throat Contribution to Permeability

The frequency distribution diagram of the throat radius contribution rate to permeability shows that, as the permeability decreases, the throat radius distribution shifts leftward relative to the distribution of high permeability, and the throat radius distribution range is narrower (Figure 9a,b). The curve peak is higher (Figure 9c). The cumulative contribution rate distribution of the throat radius to permeability indicates that a smaller throat radius contributes more significantly to permeability at lower permeability, with a larger slope in the cumulative contribution rate curve and a longer platform at the end of the frequency curve (Figure 9c). Thus, the radius of the throat plays a crucial role in the seepage capacity of the sample.

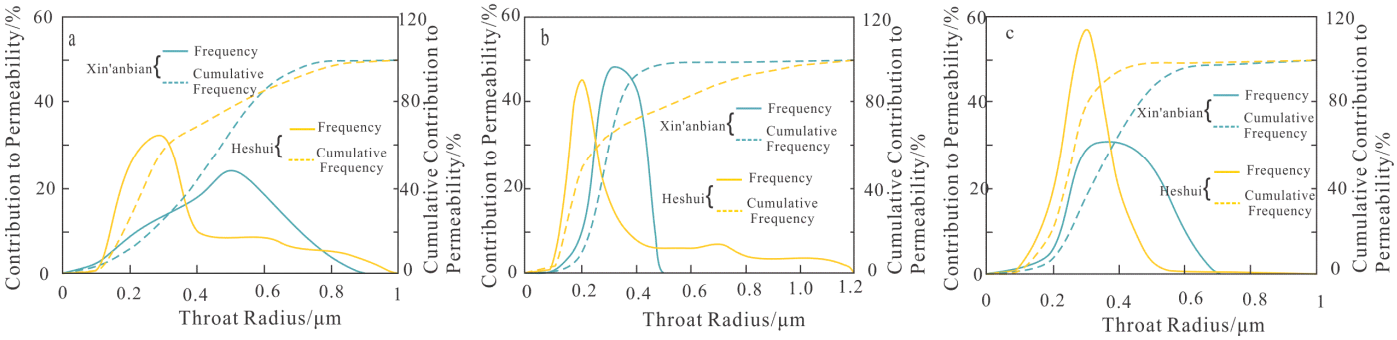

Figure 9. Contribution of size throat to permeability for different types of pore structure. (**a**) Distribution and cumulative distribution of throat radius and permeability contribution for a pore structure of Type a; (**b**) Distribution and cumulative distribution of throat radius and permeability contribution for a pore structure of Type b; (**c**) Distribution and cumulative distribution of throat radius and permeability contribution for a pore structure of Type c.

Analysis of three types of samples with the same permeability reveals that the contribution rate of the throat to permeability shows an apparent normal distribution in the Xin'anbian area (Figure 9). However, the analysis does not show a normal distribution of the contribution rate of the throat to permeability in the Heshui area. The lower the peak value of the curve and the wider the curve, the less noticeable the normal distribution of the throat contribution rate to permeability in the Heshui area is (Figure 9a). For samples of three different types of permeability, the tiny throats in the Heshui area contribute significantly to reservoir permeability (Figure 9b,c). This trend becomes more pronounced with decreasing permeability, indicating that tiny throats play a crucial role in the percolation capacity of the reservoir in the Heshui area. The pore structure complexity of the Chang 7 reservoir in the Heshui area is higher than that in the Xin'anbian area.

5. Discussion

5.1. Analysis of the Influence of Sedimentation on the Tight Reservoir Pore Structure

Previous studies have indicated that reservoir quality and pore structure differences are primarily influenced by the original sedimentary conditions and diagenesis intensity [23,24]. The Chang 7 reservoir in the Xin'anbian area is characterized by meandering river delta front subfacies, with its provenance located northeast of the basin. The main reservoir sand body is the underwater distributary channel sand body, with multi−stage thick channel sand body stacking as its primary sand body structure type. The underwater distributary channel sand body displays strong hydrodynamic conditions, well developed wedge cross−bedding (Figure 10a), and parallel bedding (Figure 10b,c) [2]. The sedimentary environment of the Chang 7 reservoir in the Heshui area, on the other hand, ranges from semi−deep to deep lake environments, with its source situated in the southwest. The main reservoir sand body is sandy clastic flow, with complex sand−body structure types. Three sand body structures have developed: multi−phase thick sand layer overlap, thick sand and thin mud interbedding, and thick sand and thin sand interbedding. The sedimentary structure at the base of the sandy debris flow exhibits a flat morphology characterized by fragmented mud gravel and a "mud−wrapped gravel" (Figure 10d) configuration transported by blocks. Additionally, block bedding (Figure 10e) and trough structures (Figure 10f) have developed, indicating the action of gravity flow during sedimentation [6]. Compared to the Xin'anbian area, the grain size of the Chang 7 reservoir in the Heshui area is finer, generally consisting of fine siltstone grains (Figure 11a). The grain size of sandstone has a significant control effect on the quality of the reservoir. Generally, an increase in grain size is typically associated with higher reservoir quality and demonstrates a positive correlation with both porosity (Figure 11a) and permeability (Figure 11b). Sedimentary hydrodynamic force affects the content of impurities, with stronger hydrodynamic forces typically corresponding to a lower impurity content and more primary intergranular pores. The sedimentary hydrodynamic force of the Chang 7 tight reservoir in the Xin'anbian area is stronger than that in the Heshui area, resulting in a better quality reservoir in the Xin'anbian area (Figure 11b).

5.2. Influence of Diagenetic Factors on Pore Structure

During the sedimentary period of Chang 7, frequent volcanic activity led to the accumulation of pyroclastic rocks, tuffs, and matrices in the reservoir, providing an essential material basis for montmorillonite formation. Illitization of montmorillonite occurs at high temperatures, and the dissolution of potassium feldspar provides a large amount of Ca^{2+}, Mg^{2+}, and Si^{4+} plasma required for the transformation. This process is a crucial source of carbonate and siliceous cementation [24]. In these two regions, the porosity (Figure 12a) and permeability (Figure 12b) display a significant negative correlation with the cementation of illite and carbonate. Specifically, when the porosity of the reservoir is less than or equal to 10%, the chlorite content exhibits a positive correlation with the porosity (Figure 12a). However, when the porosity of the reservoir exceeds 10%, the chlorite content shows a negative correlation (Figure 12a).

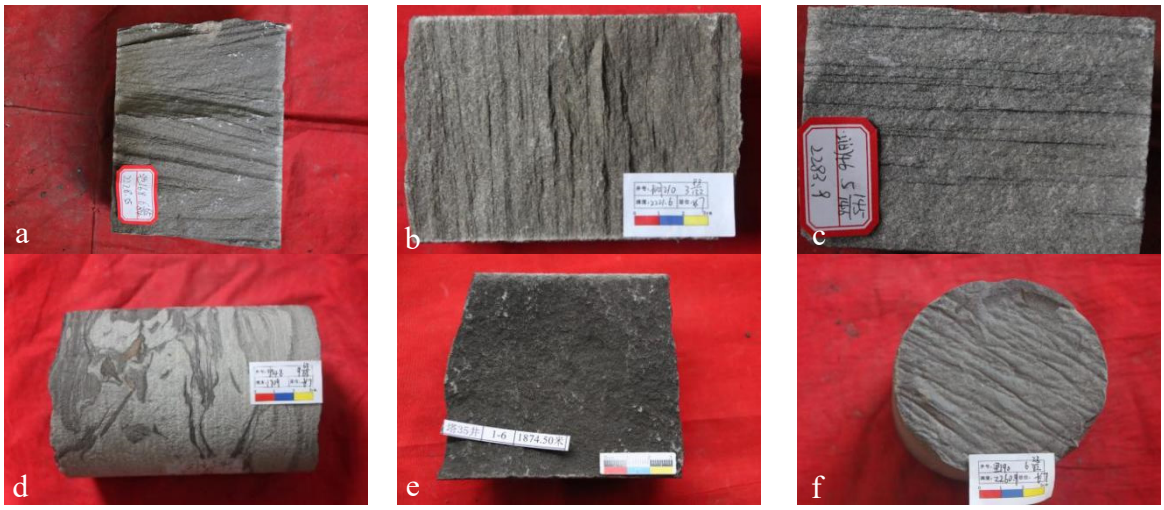

Figure 10. Main Sedimentary Structural Characteristics of Chang 7 Member tight Reservoirs. (**a**) Wedge-shaped cross-bedding, Chi 168, 2228.55 m; (**b**) Parallel bedding plate cross-bedding, Well Hu 210, 2221.6 m; (**c**) Parallel bedding, Jian 46, 2283.9 m; (**d**) Irregular mudstone tearing debris, Well Ning 148, 1709 m; (**e**) Massive oil−bearing sandstone, Ta 35, 1874.50 m; (**f**) Flute cast, Well Li 190, 2260.9 m.

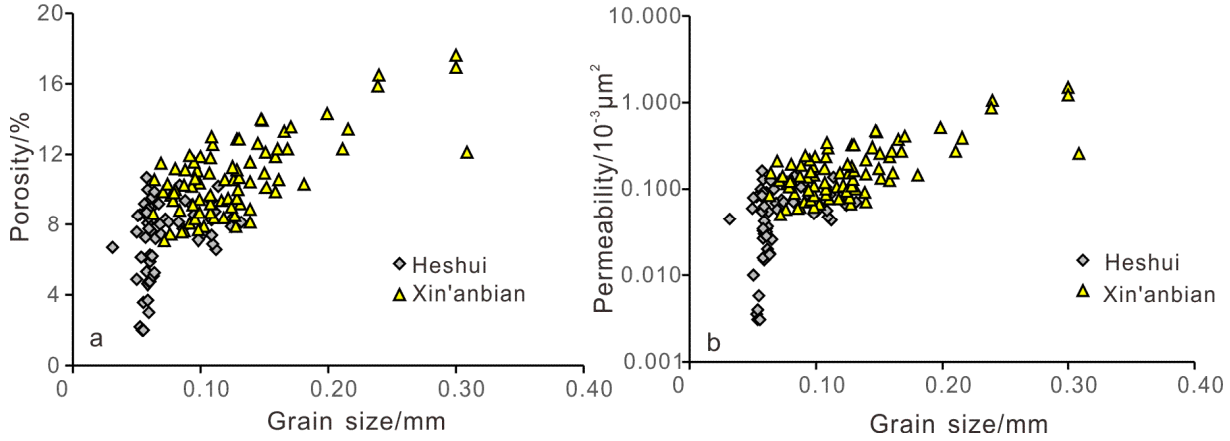

Figure 11. Relationship between grain size and physical properties of Chang 7 reservoir. (**a**) Scatter plot of particle size and porosity; (**b**) Scatter plot of particle size and permeability.

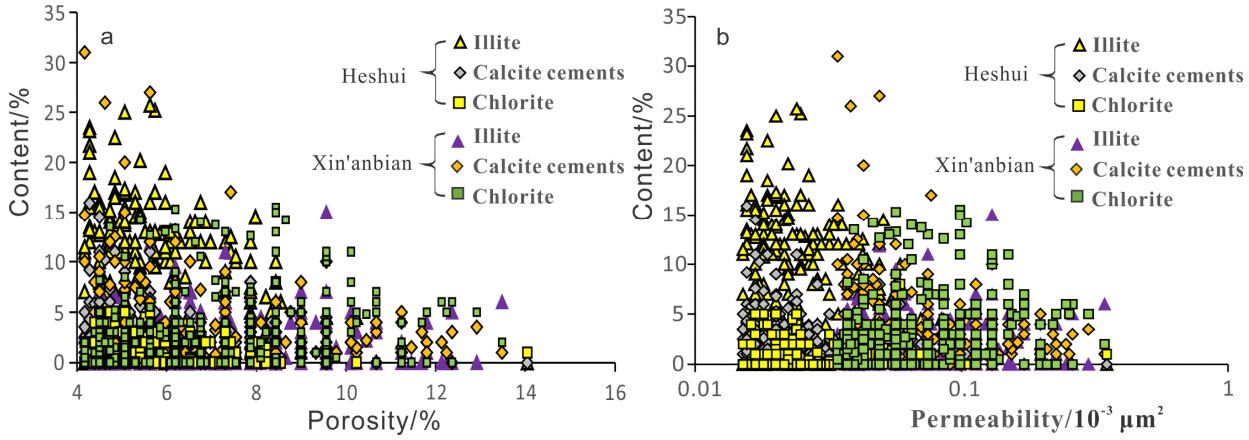

Figure 12. Plots of reservoir properties against different cement of the Chang 7 member.(**a**) Scatter plot of illite, carbonate cementation, chlorite, and porosity; (**b**) Scatter plot of illite, carbonate cementation, chlorite, and permeability. The horizontal axis employs a logarithmic scale.

The high content of illite and carbonate cementation in the Heshui area is an essential factor for the densification of its reservoirs. Potassium feldspar dissolution has made a significant contribution to reservoir dissolution [25]. Due to its location in the center of the lake basin, the Chang 7 source rock produces active acidic fluid through the pyrolysis of organic matter. Under the dissolution of acidic fluid, potassium feldspar forms many K^+ ions, essential for the illitization of montmorillonite, which consumes many K^+ ions. This dissolution reaction is the driving force behind the continuous occurrence of potassium feldspar dissolution and is the best explanation of why the illite content in the Heshui area is so high. The Xin'anbian area's tight reservoirs mainly comprise chlorite, accounting for 61.0% of the total clay minerals, followed by carbonate cement and kaolinite (Table 1). The chlorite film attached to the particle surface prevents direct contact between pore water and rock, effectively preventing excessive growth of quartz and preserving pores. The Xin'anbian chlorite aggregates' chlorite film protects part of the intergranular pores, and carbonate cementation is an essential factor in reservoir densification (Figure 12).

Strong compaction of mica or mudstone fragments can often result in plastic deformation and a significant reduction of intergranular porosity (Figure 13a). However, the presence of chlorite cement not only effectively inhibits excessive quartz growth but also positively impacts pore preservation, thereby reducing compaction. Therefore, reservoirs with chlorite cement exhibit less porosity loss due to compaction than those with more plastic minerals, such as biotite (Figure 13b). Illite and calcite cement fill pores and destroy primary porosity (Figure 13a,c). Although excessive growth of quartz can help suppress compaction, overgrowth and cementation of quartz between pores can lead to further loss of porosity (Figure 13d). The coordinates on the right side of Figure 12 provide the porosity loss rates due to compaction and cementation, with the top coordinate indicating the porosity loss rates due to cementation. Figure 13 shows that the two regions' porosity loss rates due to compaction are approximately 55%. The porosity loss rates due to cementation in the two regions are mainly between 25–50% (Figure 13).

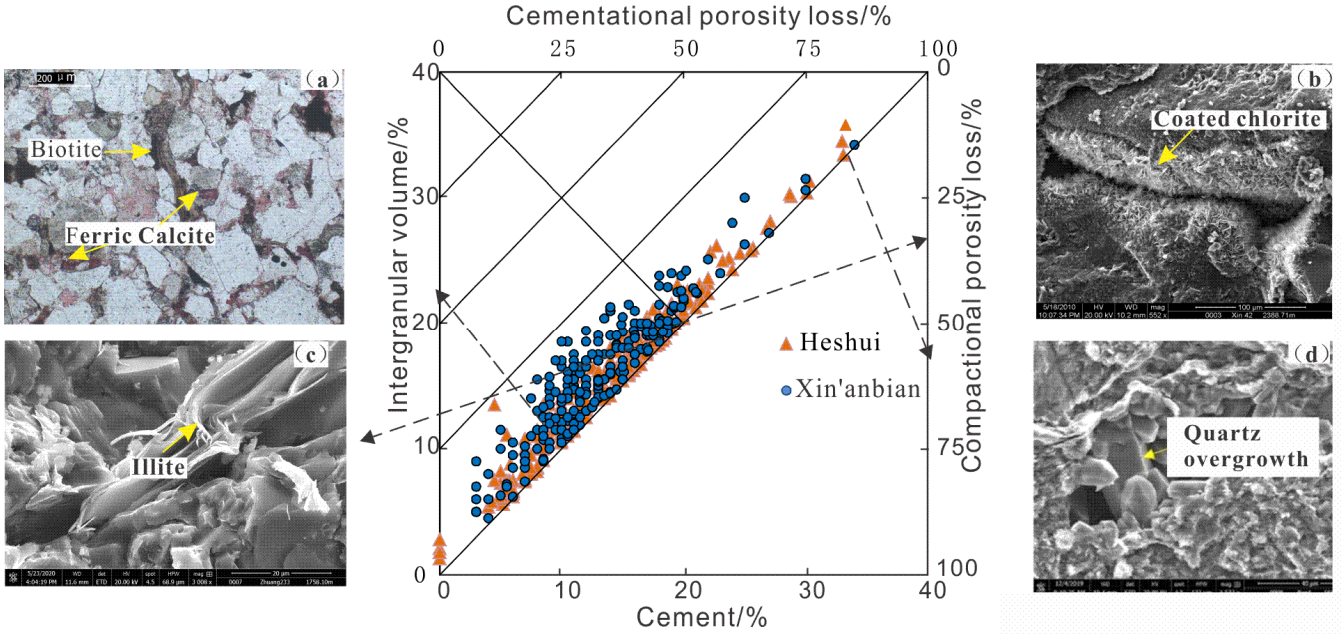

Figure 13. Intergranular pore and cement plot for Chang 7 member. (**a**) Ferric calcite, Biotite exhibiting compaction and deformation, Well Le 15, 1746.6 m; (**b**) Coated chlorite, Well Xin 42, 2388.7 m; (**c**) Illite, Well Zhuang 233, 1758.1 m; (**d**) Quartz overgrowth, Well Ban 4, 1841.5 m.

The original porosity of sandstone is determined by applying the recovery formulas of Beard and Weyle [26]. The calculation for the original porosity of the model is expressed in Equation (1):

$$\Phi_0 = 20.91 + 22.90/S_0 \quad (1)$$

where Φ_0 is the original porosity, and S_0 is the sorting coefficient of Trask.

After compaction, some of the remaining original pores will disappear due to later cementation, while others will remain. Therefore, the residual porosity Φ_1 of the reservoir after compaction includes the sum of the cement content and the original porosity preserved so far [27]:

$$\Phi_1 = \omega + (P_1 + P_2) \times P_M/P_T \quad (2)$$

where Φ_1 is the porosity after compaction, ω is the cement content, P_1 is the surface porosity of residual intergranular pores, P_2 is the surface porosity of intergranular pores, P_T is the total surface porosity, and P_M is measured porosity.

The cementation fills a part of the original pores, which can roughly equal the loss of porosity [27]. Therefore, the porosity Φ_2 of the reservoir after cementation is:

$$\Phi_2 = (P_1 + P_2) \times P_M/P_T \quad (3)$$

The increase in porosity Φ_3 by dissolution can be regarded as the ratio of the surface porosity of all dissolved pores to the total surface porosity in the corresponding measured porosity. Because the contribution rate of microfractures to the total reservoir space during diagenesis is only 1.7%, the influence is limited and is ignored in the calculation formula. Therefore, the calculation formula is [27]:

$$\Phi_3 = (P_3 + P_4 + P_5 + P_6) \times P_M/P_T \quad (4)$$

where P_3 is the surface porosity of Lithic dissolved pores, P_4 is the surface porosity of feldspar dissolved pores, P_5 is the surface porosity of carbonate dissolved pores, and P_6 is the surface porosity of matrix dissolved pores.

The sorting coefficient is a term used to describe the sorting characteristics of clastic sediments. It is defined as the ratio between the diameters of particles that correspond to 25% and 75% on the particle size distribution curve. This value is an important reference for assessing the degree of sorting within the sediment [26]. Grain size analysis results indicate that the sandstone in the Heshui area has a sorting coefficient of 1.43, while the sandstone in the Xin'anbian area has a sorting coefficient of 1.29 (Figure 14). By applying Equation (1), we calculated the initial porosity of the tight reservoir in Heshui as 36.9% and that of the Xin'anbian reservoir as 38.4%. The porosity loss due to compaction was then calculated using the formula $\Phi_0 - \Phi_1$. In the Heshui area, destructive diagenetic compaction has caused a porosity reduction of 21.48%, with an average loss rate of 58.2% (Figure 15). Similarly, in the Xin'anbian area, the porosity loss was recorded as 22.01%, with an average loss rate of 57.32%. The porosity loss due to cementation was determined using the formula $\Phi_0 - \Phi_1 - \Phi_2$. In the Heshui area, cementation has led to a porosity loss of 13.58%, while in the Xin'anbian area, the loss is 13.2% (Figure 15). The increase in porosity due to dissolution can be calculated using Equation 4, which shows an increase of 6.35% in the Heshui area and 3.99% in Xin'anbian (Figure 15). The compaction and cementation loss rate in the two regions calculated by Equations 1 to 3 are in substantial agreement with the results obtained in the model diagram shown in Figure 12. Furthermore, the current porosity values calculated using Equations 1 to 4 are consistent with those shown in Figure 5c.

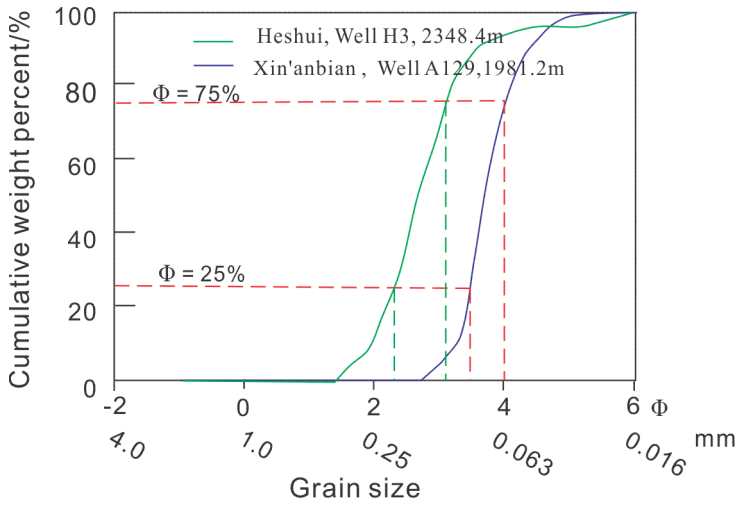

Figure 14. Cumulative graph of grain sizes (Φ).

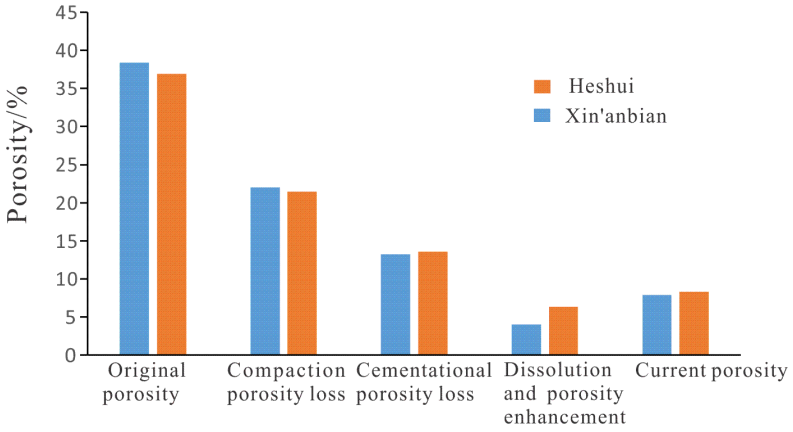

Figure 15. Effect of different diagenesis on pore evolution.

5.3. Comparison of Pore Throat Diameter Distribution in Chang 7 Tight Reservoir and Other Tight Reservoirs

The pore throat diameter distribution range of the Chang 7 tight reservoir is mainly between 50–900 nm (Figure 8). The lower limit of pore throat diameter is close to that of the Mesaverde Fm. and Travis Peak Fm., but smaller than that of the Lance Fm. and larger than that of the Bosser interval (Figure 16). The upper limit of the pore throat radius of the Chang 7 tight reservoir exceeds that of the Mesaverde Fm and Travis Peak Fm., while it is similar to that of the Lance Fm. and Bosser interval (Figure 16). Although the pore throat distribution width of the Chang 7 tight reservoir is narrower than that of the Bosser interval, it is still broader than that of other tight reservoirs, indicating significant heterogeneity in the pore throat radius distribution of the Chang 7 tight reservoir.

Numerous nanoscale pore throats exist in tight reservoirs, with pore sizes ranging from 1 to 100 nm [28,29]. According to Figure 9, nanopores constitute 15–25% of the Chang 7 tight reservoir, contributing to permeability by approximately 10%. These nanopores represent a crucial reservoir space for the Chang 7 tight reservoir, and their high specific surface area plays a pivotal role in the extraction of tight oil and gas. The study of pore throat structure enables a better understanding of the distribution characteristics of nanoscale pore throats, thereby facilitating the effective development and utilization of tight reservoir resources.

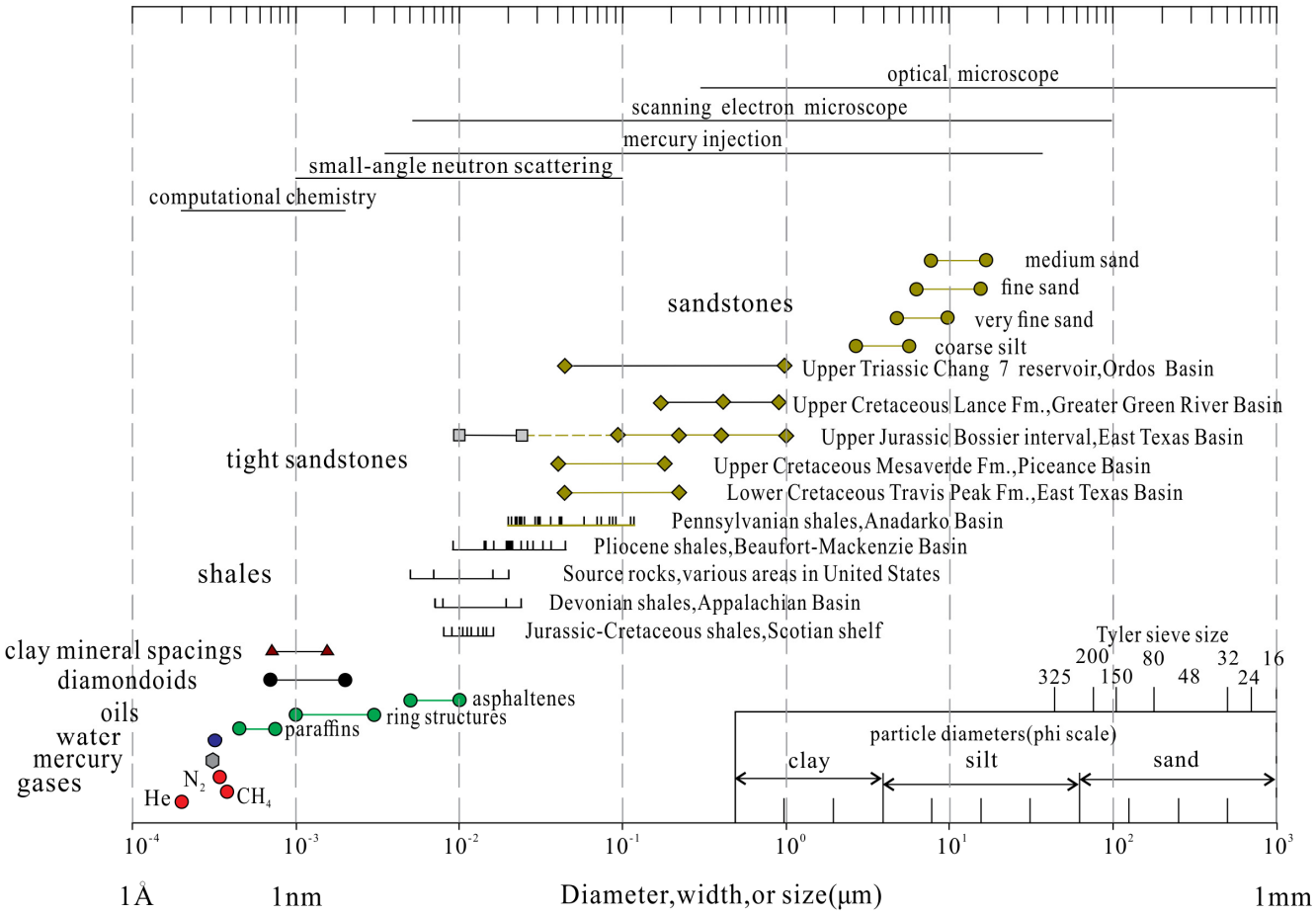

Figure 16. Sizes of molecules and pore throats in siliciclastic rocks on a logarithmic scale covering seven orders of magnitude [28]. (According to Nelson P.H., AAPG, 2009, modified, AAPG[2023] and reprinted by permission of the AAPG whose permission is required for further use.).

6. Conclusions

The pore system of the Chang 7 tight reservoir is dominated by feldspar dissolution pores and intergranular pores, with the dissolved pore throat being the most critical type. The reservoir quality is poor, and the complexity of the pore structure is high due to the tiny throats in the Heshui area, which significantly contribute to reservoir permeability. Provenance plays a vital role in controlling the difference in pore structure, with the pore structure of the reservoir with provenance from the northeast being better than that of the reservoir with provenance from the southwest.

The Heshui Reservoir exhibits low hydrodynamic forces, sediment with fine grains, and significant compaction. At the same time, the Xin'anbian Chang 7 reservoir displays high hydrodynamic forces, sediment with coarse grains, high chlorite content, and substantial dissolution. The heterogeneity in the distribution of pore throat radius is more pronounced in the Chang 7 tight reservoir than in most other tight reservoirs. Nanopores' high specific surface area plays a crucial role in producing tight oil and gas. Therefore, identifying sweet spots in both reservoirs should focus on intervals or regions characterized by type a pore structures while considering the corresponding cementation contents.

Author Contributions: Conceptualization, L.X. and Q.W.; software, L.B.; validation, L.X. and Q.W.; formal analysis, L.B.; investigation, L.B.; resources, T.Y. and Y.L.; writing—original draft preparation, L.X.; writing—review and editing, Q.W. All authors have read and agreed to the published version of the manuscript.

Funding: This project was financially supported by the National Science and Technology Major Program (2016ZX05556) and the Graduate Innovation Fund of Xi'an Shiyou University (YCS22213070).

Data Availability Statement: Not applicable.

Conflicts of Interest: The authors declare no conflict of interest.

References

1. Wei, Q.L.; Mei, J.H.; Tian, J.C.; Chen, X.; Xiao, L. Pore structure analysis of tight reservoirs in the He-8 Member of Upper Paleozoic in the southwestern Ordos Basin, China. *Interpretation* **2022**, *10*, T681–T692. [CrossRef]
2. Xiao, L.; Hu, R.; Han, Y.L.; Lei, N.; Chen, X. Characteristics of pore throat structure of Chant 7 shale oil sandstone reservoir in the western Xin'anbian area, Ordos Basin China. *J. Chengdu Univ. Technol. (Sci. Technol. Ed.)* **2022**, *49*, 284–293. (In Chinese with an English Abstract)
3. Yang, H.; Li, S.X.; Liu, X.Y. Characteristics and resource prospects of tight oil and shale oil in Ordos Basin. *Acta Pet. Sin.* **2013**, *34*, 1–11. (In Chinese with an English Abstract).
4. Fu, J.H.; Yu, J.; Xu, L.M.; Niu, X.B.; Feng, S.B.; Wang, X.J.; You, Y.; Li, T. New progress in exploration and development of tight oil in Ordos Basin and main controlling factors of large-scale enrichment and exploitable capacity. *China Pet. Explor.* **2015**, *20*, 9–19. (In Chinese with an English Abstract)
5. Fu, J.H.; Niu, X.B.; Dan, W.D.; Feng, S.B.; Liang, X.W.; Xin, H.G.; You, Y. The geological characteristics and the progress on exploration and development of shale oil in Chang 7 Member of Mesozoic Yanchang Formation, Ordos Basin. *China Pet. Explor.* **2019**, *24*, 601–614. (In Chinese with an English Abstract)
6. Fu, J.H.; Li, S.X.; Niu, X.B.; Deng, X.Q.; Zhou, X.P. Geological characteristics and exploration of shale oil in Chang7 Member of Triassic Yanchang Formation, Ordos Basin, NW China. *Pet. Explor. Dev.* **2020**, *47*, 870–883. (In Chinese with an English Abstract) [CrossRef]
7. Fu, J.H. *Theory and Technology of Tight Oil Exploration in Ordos Basin*; Science Press: Beijing, China, 2018.
8. Ehrlich, R.; Crabtree, S.J.; Horkowitz, K.O.; Horkowitz, J.P. Petrophysical and reservoir physics I: Objective classification of reservoir porosity. *AAPG Bull.* **1991**, *75*, 1547–1562.
9. Zhou, X.P.; He, Q.; Liu, J.Y.; Li, S.X.; Yang, T. Features and origin of deep-water debris flow deposits in the Triassic Chang 7 Member, Ordos Basin. *Oil Gas Geol.* **2021**, *42*, 1063–1077. (In Chinese with an English Abstract)
10. Zheng, Q.H.; Liu, Q.; Liang, X.L.; An, E.L.; Zhang, J.K.; Zheng, Y.H.; Fu, L. Sedimentary facies analysis of the Chang 7 Member of the Upper Triassic Yanchang Formation in the Ordos Basin, NW China. *J. Stratigr.* **2020**, *44*, 35–45, (In Chinese with an English Abstract).
11. Lyu, Q.Q.; Luo, S.S.; Li, M.J.; Guan, Y.L.; Zhang, J.K. Sedimentary characteristics and distribution of deep-water hybrid event beds comprising debris and turbidites: A case study of Chang7 Oil Formation in the southwest of Ordos Basin. *J. Northeast Pet. Univ.* **2020**, *44*, 69–78. (In Chinese with an English Abstract)
12. Liang, X.W.; Xian, B.Z.; Feng, S.B.; Chen, P.; You, Y.; Wu, Q.R.; Dan, W.D.; Zhang, W.S. Architecture and Main Controls of Gravity-flow Sandbodies in Chang 7 Member, Longdong Area, Ordos Basin. *Acta Sedimentol. Sin.* **2021**, *40*, 641–652. (In Chinese with an English Abstract)
13. Wang, W.; Zhu, Y.S.; Yu, C.L.; Zhao, L.; Cehn, D.Y. Pore size distribution of tight sandstone reservoir and their differential origin in Ordos Basin. *Nat. Gas Geosci.* **2019**, *30*, 1439–1450. (In Chinese with an English Abstract) [CrossRef]
14. Gao, G.; Liang, X.W.; Zhu, K.L.; Dan, W.D.; Sun, M.L.; You, Y.; Feng, S.B. Characteristics of Source-reservoir Assemblage and Hydrocarbon accumulation Model of Chang 7 Member in Ordos Basin. *Northwest. Geol.* **2021**, *54*, 198–205. (In Chinese with an English Abstract)
15. Li, G.X.; Wu, Z.Y.; Li, Z.; Chen, Q.; Xian, C.G.; Liu, H. Optimal selection of unconventional petroleum sweet spots inside continental source kitchens and actual application of three-dimensional development technology in horizontal wells: A case study of the Member 7 of Yanchang Formation in Ordos Basin. *Acta Pet. Sin.* **2021**, *42*, 736–750, (In Chinese with an English Abstract).
16. Zhang, Y.X. Source rock characterization: The dark mudstone in Chang 7 Member of Triassic, central Ordos Basin. *Oil Gas Geol.* **2021**, *42*, 1089–1097. (In Chinese with an English Abstract)
17. Liu, Q.Y.; Li, P.; Jin, Z.J.; Sun, Y.W.; Hu, G.; Zhu, D.Y.; Huang, Z.K.; Lian, X.P.; Zhang, R.; Liu, J.Y. Organic-rich formation and hydrocarbon enrichment of lacustrine shale strata: A case study of Chang 7 Member. *Sci. China Earth Sci.* **2021**, *52*, 270–290. (In Chinese with an English Abstract) [CrossRef]
18. Xiao, L.; Chen, X.; Lei, N.; Yi, T.; Guo, W.J. Characteristics and main controlling factors of shale oil reservoirs of Triassic Chang7 member in Heshui area, Ordos Basin. *Lithol. Reserv.* **2023**, *35*, 80–93. (In Chinese with an English Abstract)
19. Luo, Z.T.; Wang, Y.C. *Pore Structure of Oil and Gas Reservoir*; Science Press: Beijing, China, 1986.

20. Makeen, Y.M.; Abdullah, W.H.; Ayinla, H.A.; Hakimi, M.H.; Sia, S. Sedimentology, diagenesis and reservoir quality of the upper Abu Gabra Formation sandstones in the Fula Sub-basin, Muglad Basin, Sudan. *Sudan. Mar. Pet. Geol.* **2016**, *77*, 1227–1242. [CrossRef]
21. Ma, S.Z.; Zhang, Y.P. Study on the pore structure of tight reservoir by using method of mercury injection: A case study of the Lucaogou Formation in Jimsar sag, Junggar Basin. *Pet. Geol. Recovery Effic.* **2017**, *24*, 26–32.
22. Lai, J.; Wang, G.W.; Wang, Z.Y.; Chen, J.; Fan, X.Q. A review on pore structure characterization in tight sandstones. *Earth Sci Rev.* **2018**, *177*, 436–457. (In Chinese with an English Abstract) [CrossRef]
23. Scherer, M. Parameters influencing porosity in sandstones: A model for sandstone porosity prediction. *AAPG Bull.* **1987**, *71*, 485–491. [CrossRef]
24. Yang, T.; Cao, Y.C.; Friis, H.; Liu, K.Y.; Wang, Y.Z.; Zhou, L.L.; Zhang, S.M.; Zhang, H.N. Genesis and distribution pattern of carbonate cements in lacustrine deep-water gravity-flow sandstone reservoirs in the third member of the Shahejie Formation in the Dongying Sag, Jiyang Depression, Eastern China. *Mar. Pet. Geol.* **2018**, *92*, 547–564. [CrossRef]
25. Palhano, L.C.; Nogueira, F.C.; Marques, F.O.; Vasconcelos, D.L.; Bezerra, F.H.; Souza, J.A.; Nicchio, M.A.; Perez, Y.A.R.; Balsamo, F. Influence of hydrothermal silicification on the physical properties of a basin-boundary fault affecting arkosic porous sandstones, Rio do Peixe Basin, Brazil. *Mar. Pet. Geol.* **2023**, *148*, 106062. [CrossRef]
26. Beard, D.C.; Wely, P.K. Influence of texture on porosity and permeability of unconsolidated sand. *AAPG Bull.* **1973**, *57*, 349–369.
27. Liao, M.G.; Li, H.; Nan, J.X.; Liao, J.J.; Yao, J.L. Diagenesis and Quantitative Analysis of Pore Evolution of He 8 Member Reservoir in Sulige Region. *Speicial Oil Gas Reserv.* **2017**, *24*, 15–20.
28. Nelson, P.H. Pore-throat sizes in sandstones, tight sandstones, and shales. *AAPG Bull.* **2009**, *93*, 329–340. [CrossRef]
29. Wu, S.T.; Zhu, R.K.; Zhi, Y.; Mao, Z.G.; Cui, J.W.; Zhang, X.X. Distribution and characteristics of lacustrine tight oil reservoirs in China. *J. Asian Earth Sci.* **2019**, *178*, 20–36. [CrossRef]